Power Oscillation Damping Using FACTS Devices: Modal Controllability, Observability in Local Signals, and Location of Transfer Function Zeros

U. P. Mhaskar and A. M. Kulkarni

***Abstract*—Modal controllability, observability, and transfer function zeros play an important role in the selection of candidate locations and feedback signals for flexible ac transmission systems (FACTS)-based power swing damping controllers. This paper investigates location of zeros of the transfer function corresponding to FACTS devices and certain local feedback signals. Signals synthesized from locally measured signals are derived that can give good pole-zero separation. It is also shown that relative modal controllability of FACTS controllers at various locations can be directly inferred from relative modal observability in certain signals at those locations. These signals are identified for various FACTS devices. Case studies using detailed model are used to validate the results.**

***Index Terms*—Flexible ac transmission systems (FACTS), power system control, power system dynamic stability.**

I. Introduction

THE PROBLEM of low-frequency power swings is a matter of concern for power engineers. The traditional solution to this problem is the use of power system stabilizers (PSSs). The advent of high-power electronic equipment to improve utilization of transmission capacity, as envisaged in the concept of flexible ac transmission systems (FACTS) controllers, provides a system planner with additional leverage to improve the stability of a system. FACTS do not indicate a particular controller but a host of controllers that the system planner can choose based on both technical considerations and a cost benefit analysis. FACTS controllers like static var compensator (SVC), static synchronous compensator (STATCOM), thyristor controlled series compensator (TCSC), static synchronous series compensator (SSSC), and unified power flow controller (UPFC) can provide variable shunt and/or series compensation [1].

A FACTS device should have an adequate margin of variable compensation for effective damping of power swings. Therefore, while planning for FACTS controllers, an important consideration is the "damping effect per MVAR" [2] or the "control cost." A damping controller may be an auxiliary controller that is present in addition to another controller (like a voltage regulator in a STATCOM or SVC). Some FACTS installations have also been conceived primarily for power swing damping improvement [3]. In such cases, the damping controller function utilizes the whole control range (including transient over-rating capability, if available).

A higher *controllability* of a critical mode results in a smaller variable compensation requirement for a given modal damping performance. Controllability is dependent on the location and nature of the FACTS device under consideration.

There exists some flexibility in the choice of a feedback signal in a damping controller. While a locally available signal or a signal synthesized from local measurements is preferable, the use of remote or "global" signals is technologically feasible [4], [5]. *Observability* of a critical mode in a signal is an important consideration in the choice of a feedback signal. However, choice of a "good" signal requires examination of several aspects, including the effect on modes other than the swing mode of interest.

A *residue* is a measure dependent on *both* modal observability in the feedback signal and modal controllability (it is a normalized product of modal observability and controllability). A higher magnitude of residue implies a higher sensitivity of the corresponding eigenvalue to controller gain. While residues indicate the movement of eigenvalues for small gain, the large gain behavior is determined by the transfer function zeros. It is important to have good separation between critical poles and zeros in order to obtain adequate eigenvalue movement with increasing gain. Good separation can be achieved by appropriate choice of feedback signals or by retuning existing controllers in the system [6].

Given the flexibility in choice of a feedback signal, it may not be appropriate to choose effective locations based on modal observability in a predecided feedback signal or residue of the corresponding transfer function. On the other hand, modal controllability is a good indicator for choosing effective locations, since it gives an idea of the leverage of a FACTS controller on a mode [7] and has a bearing on the equipment size. However, modal observability has been implicitly used in the previous literature to screen candidate locations. Locations at which large swings in current and voltage are observable are considered to be the "natural" candidates for series and shunt controllers, respectively. Tie-lines in which interarea mode power swings are large are considered to be good locations for placing series FACTS devices (for damping an interarea mode). Similarly, the largest amplitude points of the mode shape of the bus voltages are considered to be good candidate buses for shunt reactive FACTS

Manuscript received December 13, 2004; revised May 25, 2005. This work was carried out at IIT Bombay and supported by the Department of Science and Technology (DST), Gov. of India, under Scheme no. III-5(33)/99-ET. Paper no. TPWRS-00642-2004.

U. P. Mhaskar is with GE India Technology Center Pvt. Ltd., Bangalore-560066, India.

A. M. Kulkarni is with the Department of Electrical Engineering, Indian Institute of Technology Bombay, Powai-400076, Mumbai, Maharashtra, India (e-mail:anil@ee.iitb.ac.in).

Digital Object Identifier 10.1109/TPWRS.2005.856983

devices [8]. Motivated by these issues, we investigate the following in this paper:

1) *Location of zeros of transfer function corresponding to FACTS devices and local signals:*
   It is shown using classical model that zeros and poles are interleaved if local signals like voltage magnitude (for a STATCOM damping controller) and current magnitude (for SSSC) are used. Interestingly, the pole-zero interleaving property has been recognized in several other analogous physical systems [9]. Suitable zero placement can be obtained by modifying local signals. The required modifications are suggested by the analysis carried out in the paper.
2) *Duality between the controllability of swing mode(s) by using shunt/series FACTS devices at various locations and the observability of the swing mode(s) in certain signals like voltage/current at those locations:*
   It has been shown by Samuelsson [10] that such a duality exists for shunt real power modulation and bus frequency. This paper generalizes this result to a wider set of FACTS devices and signals. For example, it is proved using classical model that relative modal controllability corresponding to the control inputs (e.g., shunt reactive current for STATCOMs, series reactive voltage for SSSCs), can be inferred from relative modal observability corresponding to the measured signals (bus voltage magnitude at STATCOM locations, line current magnitude at SSSC locations).

The result pertaining to zero locations is demonstrated using SSSC for simplified and detailed models. With detailed models, it is also seen that the duality result is a good approximation for series reactive and shunt real power modulating FACTS devices, although it is not valid for shunt reactive power and series real power devices.

A. List of Main Symbols

δ	Generator rotor angle.
ω	Generator rotor speed.
ω_B	Machine base speed.
ϕ	Bus voltage phase angle.
ζ	Line current phase angle.
I	Line current magnitude.
I_R	Shunt injected reactive current (positive when capacitive).
V	Bus voltage magnitude.
V_R	Series injected reactive voltage (voltage in quadrature with current: positive when inductive).
P_{sh}	Shunt injected real power.
P_{ser}	Series injected real power.
Q_{sh}	Shunt injected reactive power.
Q_{ser}	Series injected reactive power.
Xt_{ser}	Series connected reactance.
Bs_{sh}	Shunt connected susceptance.
H	Generator inertia constant.
	The subscript "o" denotes equilibrium value.
	The prefix Δ denotes small deviation from equilibrium.
	Bold characters denote vectors.

II. Linearized Analysis of a Power System

The electromechanical modes in a system are highlighted by considering the classical model of generators. In addition, the following assumptions simplify the analysis.

1) The losses in the transmission lines are neglected.
2) Load active power is constant, and reactive power is of constant susceptance type.
3) Generators are represented by classical model. Prime mover input is held constant.
4) FACTS devices can implement a control order for changing real or reactive power injection in a very short time as compared to the period associated with power swings. Therefore, the "plant dynamics" associated with FACTS devices is neglected.

The linearized swing equations along with the real and reactive power balance equations for all nodes and for the branches in which series compensation is present can be formulated as follows (see the Appendix):

$$\begin{bmatrix} \boldsymbol{\Delta\dot{\delta}} \\ -M\boldsymbol{\Delta\dot{\omega}} \\ \boldsymbol{\Delta P_{sh}} \\ \boldsymbol{\Delta I_R} \\ \boldsymbol{\Delta P_{ser}} \\ \boldsymbol{\Delta V_R} \end{bmatrix} = J \begin{bmatrix} \boldsymbol{\Delta\delta} \\ \boldsymbol{\Delta\omega} \\ \boldsymbol{\Delta\phi} \\ \boldsymbol{\Delta V} \\ \boldsymbol{\Delta\zeta} \\ \boldsymbol{\Delta I} \end{bmatrix} \tag{1}$$

where the structure of J is as follows:

$$J = \begin{bmatrix} [0] & I & [0] & [0] & [0] & [0] \\ A_{11} & [0] & A_{12} & A_{13} & A_{14} & A_{15} \\ A_{21} & [0] & A_{22} & A_{23} & A_{24} & A_{25} \\ A_{31} & [0] & A_{32} & A_{33} & A_{34} & A_{35} \\ A_{41} & [0] & A_{42} & A_{43} & A_{44} & A_{45} \\ A_{51} & [0] & A_{52} & A_{53} & A_{54} & A_{55} \end{bmatrix} \tag{2}$$

and M is a diagonal matrix with ith diagonal element equal to $2H_i/\omega_B$.

The following relationship holds true for the submatrices of J (see the Appendix):

$$A_{ij} = A_{ji}^T, \qquad i,j = 1,\ldots,5. \tag{3}$$

The controllable inputs are

$$\mathbf{u} = [\boldsymbol{\Delta P_{sh}}^T \quad \boldsymbol{\Delta I_R}^T \quad \boldsymbol{\Delta P_{ser}}^T \quad \boldsymbol{\Delta V_R}^T]^T$$

while the observable quantities are

$$\mathbf{y} = \left[\boldsymbol{\Delta\phi}^T \quad \boldsymbol{\Delta V}^T \quad \boldsymbol{\Delta\zeta}^T \quad \boldsymbol{\Delta I}^T\right]^T.$$

Therefore, (1) can be written in state–space form as follows:

$$\begin{bmatrix} \boldsymbol{\Delta\dot{\delta}} \\ \boldsymbol{\Delta\dot{\omega}} \end{bmatrix} = A \begin{bmatrix} \boldsymbol{\Delta\delta} \\ \boldsymbol{\Delta\omega} \end{bmatrix} + B\mathbf{u} \tag{4}$$

$$\mathbf{y} = C \begin{bmatrix} \boldsymbol{\Delta\delta} \\ \boldsymbol{\Delta\omega} \end{bmatrix} + D\mathbf{u}. \tag{5}$$

where

$$A = \begin{bmatrix} [0] & I \\ -M^{-1}A_r & [0] \end{bmatrix} \tag{6}$$

$$A_r = A_{11} - [\,A_{12} \quad A_{13} \quad A_{14} \quad A_{15}\,] J_r \begin{bmatrix} A_{21} \\ A_{31} \\ A_{41} \\ A_{51} \end{bmatrix} \tag{7}$$

$$B = -M^{-1}\begin{bmatrix} [0] \\ B_\omega \end{bmatrix} = -M^{-1}\begin{bmatrix} [0] & [0] & [0] & [0] \\ A_{12} & A_{13} & A_{14} & A_{15} \end{bmatrix} J_r \tag{8}$$

$$C = -[\,C_\delta \quad [0]\,] = -J_r \begin{bmatrix} A_{21} & [0] \\ A_{31} & [0] \\ A_{41} & [0] \\ A_{51} & [0] \end{bmatrix} \tag{9}$$

$$J_r = \begin{bmatrix} A_{22} & A_{23} & A_{24} & A_{25} \\ A_{32} & A_{33} & A_{34} & A_{35} \\ A_{42} & A_{43} & A_{44} & A_{45} \\ A_{52} & A_{53} & A_{54} & A_{55} \end{bmatrix}^{-1} = D. \tag{10}$$

A. Eigen-Analysis

The right and left eigenvectors of A, corresponding to an eigenvalue λ_i, are defined as follows:

$$\lambda_i \mathbf{e_i} = A\mathbf{e_i} = \begin{bmatrix} [0] & I \\ -M^{-1}A_r & [0] \end{bmatrix} \begin{bmatrix} \mathbf{e_{\delta i}} \\ \mathbf{e_{\omega i}} \end{bmatrix} \tag{11}$$

$$\mathbf{f_i}^T \lambda_i = \mathbf{f_i}^T A = [\,\mathbf{f}_{\boldsymbol{\delta i}}^T \quad \mathbf{f}_{\boldsymbol{\omega i}}^T\,] \begin{bmatrix} [0] & I \\ -M^{-1}A_r & [0] \end{bmatrix}. \tag{12}$$

From the above equations, we obtain

$$\lambda_i \mathbf{e_{\delta i}} = \mathbf{e_{\omega i}} \tag{13}$$

$$\lambda_i \mathbf{e_{\omega i}} = -M^{-1}A_r \mathbf{e_{\delta i}}. \tag{14}$$

Therefore

$$\lambda_i^2 (M^{1/2}\mathbf{e_{\delta i}}) = -(M^{-1/2}A_r M^{-1/2})(M^{1/2}\mathbf{e_{\delta i}}). \tag{15}$$

The matrix $(M^{-1/2}A_rM^{-1/2})$ is symmetric since A_r is symmetric. Therefore, its eigenvalues μ_i are real. Moreover, for feasible operating points, $(M^{-1/2}A_rM^{-1/2})$ is positive semidefinite. Therefore, since λ_i^2 is an eigenvalue of $-(M^{-1/2}A_rM^{-1/2})$, it follows that $\lambda_i = \pm j\sqrt{\mu_i}$.

Due to symmetry of A_r we can also see that

$$\lambda_i^2 (M^{-1/2}\mathbf{f_{\omega i}}) = -(M^{-1/2}A_r M^{-1/2})(M^{-1/2}\mathbf{f_{\omega i}}). \tag{16}$$

Therefore, we can choose

$$(M^{-1/2}\mathbf{f_{\omega i}}) = h_i (M^{1/2}\mathbf{e_{\delta i}}) \tag{17}$$

from which we obtain the following relationship between the left and right eigenvectors:

$$\mathbf{f_i} = \begin{bmatrix} \mathbf{f_{\delta i}} \\ \mathbf{f_{\omega i}} \end{bmatrix} = h_i \begin{bmatrix} \lambda_i M \mathbf{e_{\delta i}} \\ M \mathbf{e_{\delta i}} \end{bmatrix} \tag{18}$$

where h_i is a scalar constant that can be chosen arbitrarily.

B. Transfer Function Zeros

Let us investigate the location of transfer function zeros when the following input–output pair is chosen:

$$u = P\mathbf{u} \tag{19}$$

$$y = P\mathbf{y}. \tag{20}$$

For simplicity, P is chosen as a row vector with a single nonzero entry whose value is 1. An example of an input–output pair is $u = I_{Rj}$ and $y = V_j$, where j denotes the bus number.

For a control law : $u = ky$, the resulting state equation becomes

$$\begin{bmatrix} \boldsymbol{\Delta\dot{\delta}} \\ \boldsymbol{\Delta\dot{\omega}} \end{bmatrix} = A \begin{bmatrix} \boldsymbol{\Delta\delta} \\ \boldsymbol{\Delta\omega} \end{bmatrix} + BP^T u \tag{21}$$

$$y = P\mathbf{y} = PC \begin{bmatrix} \boldsymbol{\Delta\delta} \\ \boldsymbol{\Delta\omega} \end{bmatrix} + PDP^T u. \tag{22}$$

Therefore

$$\begin{bmatrix} \boldsymbol{\Delta\dot{\delta}} \\ \boldsymbol{\Delta\dot{\omega}} \end{bmatrix} = \left(A + \frac{kBP^TPC}{1 - kPDP^T} \right) \begin{bmatrix} \boldsymbol{\Delta\delta} \\ \boldsymbol{\Delta\omega} \end{bmatrix}. \tag{23}$$

Thus, we have

$$A_k = \left(A + \frac{kBP^TPC}{1 - kPDP^T} \right) = \begin{bmatrix} [0] & I \\ -M^{-1}A_{rk} & [0] \end{bmatrix} \tag{24}$$

where

$$A_{rk} = A_r - \frac{kB_\omega P^T PC_\delta}{1 - kPDP^T}. \tag{25}$$

If we let k tend to ∞, we will obtain

$$A_{r\infty} = A_r + \frac{B_\omega P^T PC_\delta}{PDP^T}. \tag{26}$$

Note that due to (4), (8), and (9)

$$B_\omega = C_\delta^T. \tag{27}$$

By writing $M^{-1/2}B_\omega P^T = q$ and $\sigma = 1/PDP^T$, we can write

$$M^{-1/2}A_{r\infty}M^{-1/2} = M^{-1/2}A_rM^{-1/2} + \sigma qq^T. \tag{28}$$

If eigenvalues of $(M^{-1/2}A_rM^{-1/2})$ are $\mu_1 \geq \mu_2 \geq \cdots \mu_n$ and the eigenvalues of $(M^{-1/2}A_{r\infty}M^{-1/2})$ are $\xi_1 \geq \xi_2 \geq \cdots \xi_n$, then [11]

1) if $\sigma \geq 0$

$$\mu_i \leq \xi_i \leq \mu_{i-1}, \qquad i = 2:n$$
$$\mu_2 \leq \xi_1 \leq \mu_1 + \sigma q^T q.$$

2) if $\sigma \leq 0$

$$\mu_{i+1} \leq \xi_i \leq \mu_i, \qquad i = 1:n-1$$
$$\mu_n + \sigma q^T q \leq \xi_n \leq \mu_n.$$

Since $A_{r\infty}$ is obtained by allowing k to tend to infinity, the eigenvalues of $(M^{-1/2}A_{r\infty}M^{-1/2})$ are related to the zeros (z_i) of the transfer function between u and y by the relationship $z_i = \pm j\sqrt{\xi_i}$. Thus, one sees that poles and zeros are *interleaved*. If

$PDP^T \neq 0$, then all the zeros are finite. The bound on the value of ξ_1 or ξ_n is dependent on the magnitude of $\sigma q^T q$.

If instead of using $y = P\mathbf{y}$, we use $y' = P\mathbf{y} - \gamma PDP^T\mathbf{u}$ as the feedback signal, then it is clear that $\sigma' = 1/(1-\gamma)PDP^T$, which equals ∞ when $\gamma = 1$. This results in a pair of zeros with magnitude equal to ∞. This is desirable from the point of view of having a good pole zero separation. By making the modification, we neutralize the effect of D.

Thus, it is desirable to use the signals that are of the form $V - \alpha I_R$, $I - \alpha V_R$, $\phi - \alpha P_{sh}$ and $\zeta - \alpha P_{ser}$ in conjunction with the inputs I_R, V_R, P_{sh}, and P_{ser}, respectively, where α is appropriately chosen.

C. Modal Controllability and Observability

The modal controllability vector is defined as

$$\boldsymbol{\beta_i} = (\mathbf{f_i}^T B)^T = B^T \mathbf{f_i}. \tag{29}$$

The modal observability vector is defined as

$$\boldsymbol{\gamma_i} = C\mathbf{e_i}. \tag{30}$$

From (18) and (27), we obtain

$$\boldsymbol{\beta_i} = h_i \boldsymbol{\gamma_i}. \tag{31}$$

Thus, the modal controllability and observability vectors are parallel. The result of (31) shows that the *relative* modal controllability using various inputs defined by $\mathbf{u}$ can be inferred from the *relative* modal observability in the signals of $\mathbf{y}$. For example, if the relative modal controllability using series reactive voltage control (by SSSCs) at two different locations is desired, it can be obtained directly from the relative observability of the mode in the current magnitude deviations at *those* locations. The result also shows that different devices like STATCOM and SSSC can also be compared by the observability of the mode in the appropriate local signals. The structure and symmetry of the submatrices A_{ij} are unchanged if the inputs and outputs are as follows:

$$\mathbf{u}' = [\,\mathbf{\Delta P_{sh}}^T \quad \mathbf{\Delta Q_{sh}}^T \quad \mathbf{\Delta P_{ser}}^T \quad \mathbf{\Delta Q_{ser}}^T\,]^T$$
$$\mathbf{y}' = \left[\,\mathbf{\Delta\phi}^T \quad \frac{\mathbf{\Delta V}}{\mathbf{V_o}}^T \quad \mathbf{\Delta\zeta}^T \quad \frac{\mathbf{\Delta I}}{\mathbf{I_o}}^T\,\right]^T$$

or

$$\mathbf{u}'' = [\,\mathbf{\Delta P_{sh}}^T \quad \mathbf{\Delta Bs_{sh}}^T \quad \mathbf{\Delta P_{ser}}^T \quad \mathbf{\Delta Xt_{ser}}^T\,]^T$$
$$\mathbf{y}'' = \left[\,\mathbf{\Delta\phi}^T \quad \mathbf{V_o\Delta V}^T \quad \mathbf{\Delta\zeta}^T \quad \mathbf{I_o\Delta I}^T\,\right]^T.$$

Consequently, the same result can be derived for these set of inputs and outputs. The modal controllability for the set of inputs corresponding to reactive powers is pertinent if the relative control cost is to be estimated in terms of "damping *per MVAr*." The controllable inputs, the corresponding dual signals, and the relevant FACTS devices are summarized in Table I.

Since the relative modal observability in bus frequency ($d\phi/dt$) at various locations is the same as that in phase angle (ϕ), it follows that P_{sh} and bus frequency are also a dual pair—this was first recognized by Samuelsson in [10].

TABLE I
DUAL INPUTS AND SIGNALS

Input	Signal	FACTSd evices
ΔP_{sh}	$\Delta\phi$	STATCOM with energy source
ΔQ_{sh}	$\frac{\Delta V}{V_o}$	STATCOM, SVC
ΔI_R	ΔV	STATCOM
ΔBs_{sh}	$V_o\Delta V$	SVC
ΔP_{ser}	$\Delta\zeta$	SSSC with energy source
ΔQ_{ser}	$\frac{\Delta I}{I_o}$	SSSC,T CSC
ΔV_R	ΔI	SSSC
ΔXt_{ser}	$I_o\Delta I$	TCSC

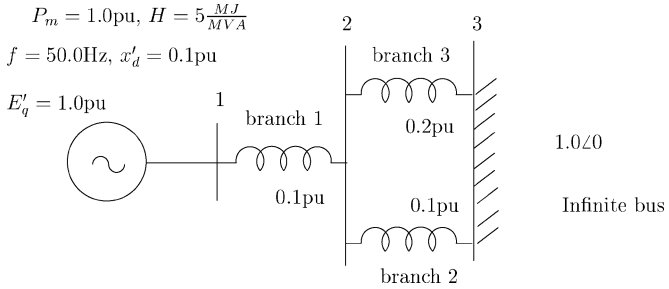

Fig. 1. Single machine infinite bus system.

D. Residue Angle

The residue corresponding to the ith eigenvalue of the transfer function corresponding to u and y of (20) is given by

$$\rho_i = \frac{\boldsymbol{\beta_i}^{\mathbf{T}} P^T P \boldsymbol{\gamma_i}}{\mathbf{f_i}^T \mathbf{e_i}} \tag{32}$$
$$= \frac{\boldsymbol{\beta_i}^{\mathbf{T}} P^T P \boldsymbol{\beta_i}}{2\lambda_i \mathbf{e}_{\boldsymbol{\delta i}}^T M \mathbf{e_{\delta i}}} \tag{33}$$
$$\tag{34}$$

$\mathbf{e_{\delta i}}$, and consequently $\boldsymbol{\beta_i}$, can be be chosen to be real since the matrix $(M^{-1/2}A_r M^{-1/2})$ is symmetric. Moreover, since λ_i is imaginary, it follows that $\angle\rho_i = -90^\circ$ for the eigenvalues on the positive imaginary axis. This implies that in order to obtain initial movement of eigenvalues toward the negative real direction, a damping controller will have to provide a lead of 90° between y and $(-u)$ at swing mode frequencies.

E. Illustrative Example

Consider a single machine connected to an infinite bus by a network of three branches.

There is only one undamped swing mode in this system since classical model of a machine is used. The system along with the relative magnitudes of the reactance of branches is shown in Fig. 1.

The zero locations for SSSC in the three branches (considered one at a time), with $u = V_{Ri}$ and $y = I_i$, $i = 1$ to 3, are shown in Fig. 2. Note that in this case, $\sigma \leq 0$. For SSSC in branch 3, the zero is relatively close to the pole. We can shift this zero location to a more appropriate value by choosing the output to be $y' = I_3 - \gamma PDP^T V_{R3}$ (see Fig. 3).

A damping controller using a control law $u(s) = -(ks/(0.01s+1)^2)y(s)$ is unable to achieve much damping because of the zero near the pole that causes it to "turn back" (see Fig. 4). However, an improved damping performance with

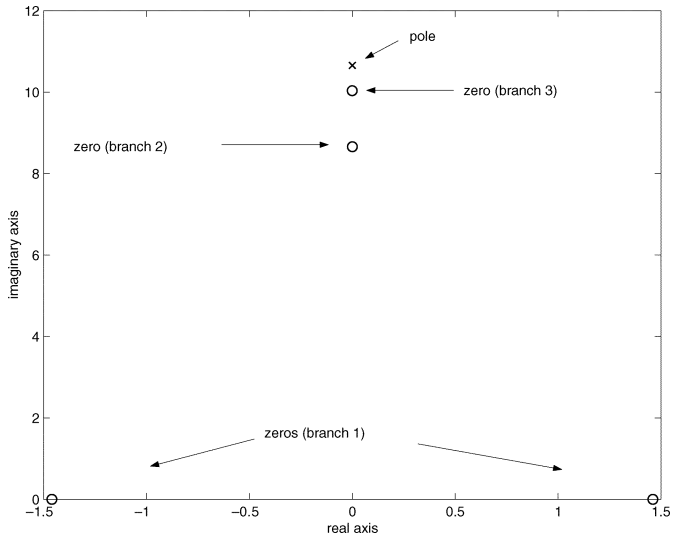

Fig. 2. Pole–zero locations for SSSC in various branches.

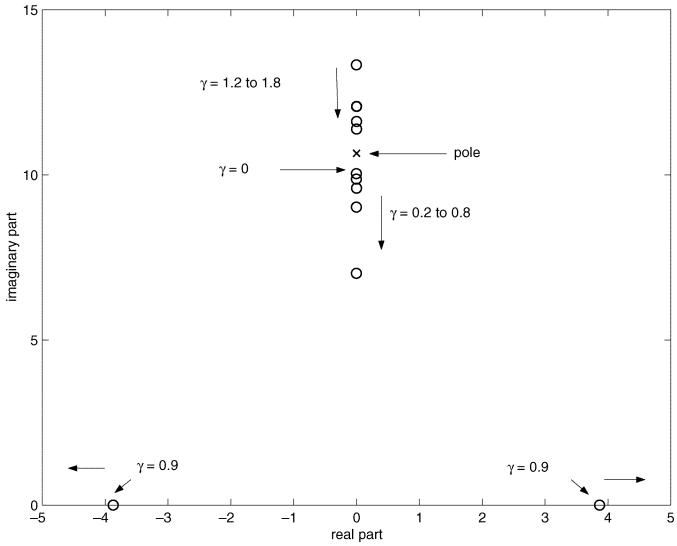

Fig. 3. Zero locations for various values of γ : SSSC in branch 3.

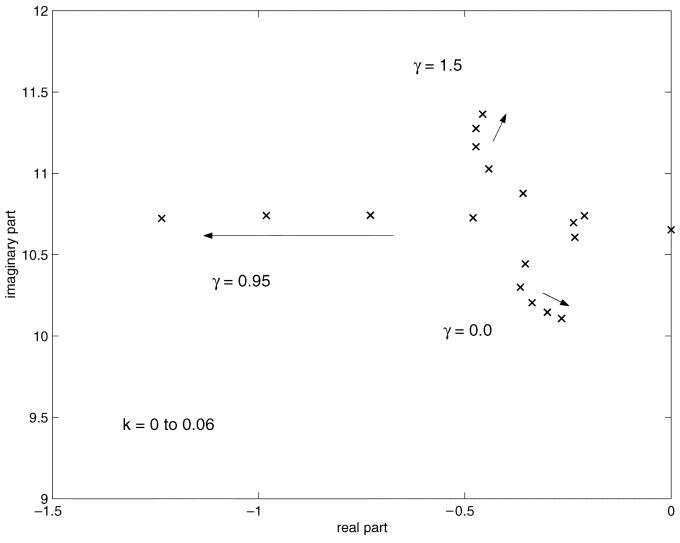

Fig. 4. Root loci with increasing gain : Various values of γ : SSSC in branch 3.

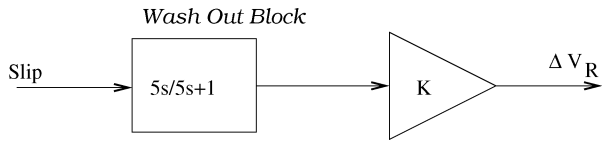

Fig. 5. Damping controller structure.

increasing gain can be achieved by using the modified feedback signal y' with an appropriate value of γ.

Suppose we wish to compare the relative modal controllability of the swing mode using series reactive voltage control (SSSC). It is obvious that the modal observability of the swing in the dual signal (current magnitude in the three branches) is in the ratio 1 : 2/3 : 1/3—due to relative magnitudes of reactances.

As per the duality result, modal controllability using reactive voltage control is also in the same ratio.

Since modal controllability is intimately related to the control effort, we expect that the range of vernier control of a SSSC required will be in the inverse ratio, i.e., 1 : 3/2 : 3 *for the same damping performance*. To show this, consider (one at a time) reactive voltage-based damping controllers on the three branches. For simplicity, the damping controller structure is chosen to be common, with the machine slip as the input (see Fig. 5). The gains are chosen such that damping ratio achieved for the swing mode is the same for all cases.

The response for a pulse disturbance of -0.1 pu in the infinite bus voltage is shown in Fig. 6. Note that the damping ratio for all three cases is the same. The maximum range (deviation) of reactive voltage compensation required for the same damping ratio is in the inverse ratio of the modal observability of current at those locations, as expected.

III. Case Studies Using Detailed Models

The results presented in the previous section are true only for classical model. Unfortunately, the precise relationship between the eigenvectors [see (18)] cannot be obtained when detailed models and AVR are considered. Thus, we have to rely on numerical tests to check the approximate validity for detailed models. This study is carried out in this section.

It should be noted there is no unique choice of $\mathbf{f_i}$ and $\mathbf{e_i}$ (an eigenvector multiplied by a scalar value is also an eigenvector). Therefore, the vectors $\boldsymbol{\gamma_i}$ and $\boldsymbol{\beta_i}$ are not unique, and only relative component values of these vectors are of importance. However, in the results presented in this section, h_i is chosen such that

$$\mathbf{f_i^T e_i} = 1. \tag{35}$$

Note that with this choice of $\mathbf{f_i}$, the product of the modal controllability for an input and the modal observability for the output also equals the *residue* of the corresponding transfer function.

We consider a three-machine system (data adapted from [12]) as shown in Fig. 7. FACTS devices are considered at each branch and node of the network. The case studies are carried out using a detailed generator model (field and damper winding modeled) [13], static exciter with AVR, lossy lines, and constant impedance loads. There are two swing modes in this system.

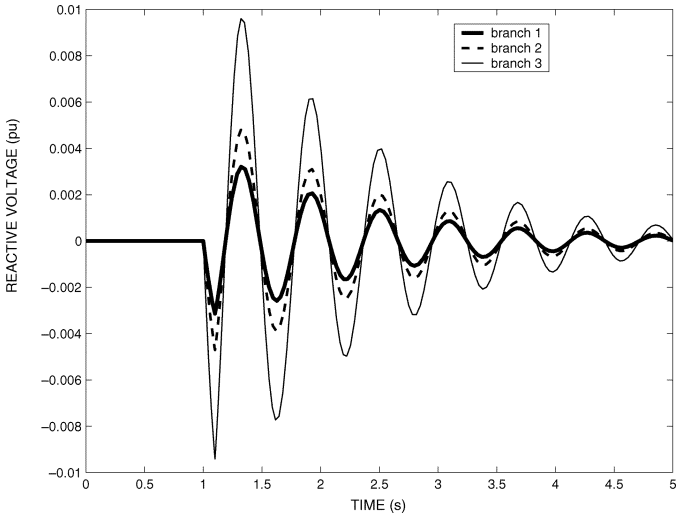

Fig. 6. Reactive voltage modulation for obtaining same damping performance.

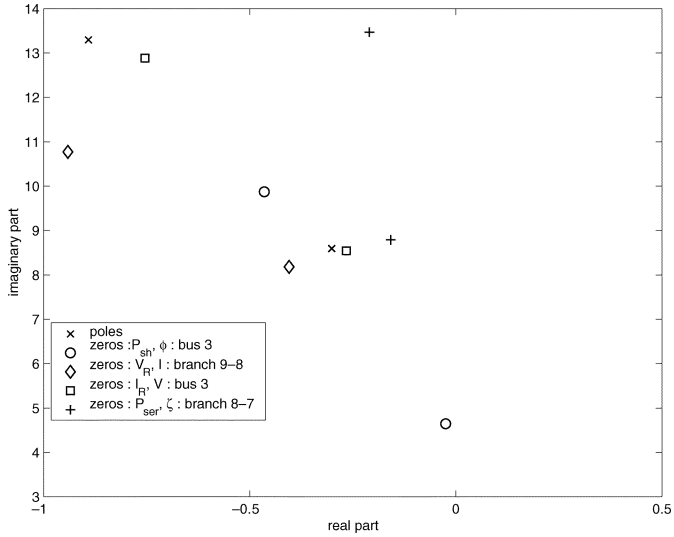

Fig. 8. Pole–zero locations : Three-machine system.

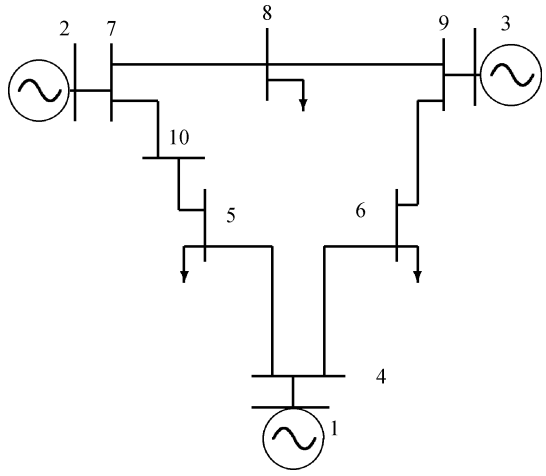

Fig. 7. Three-machine system.

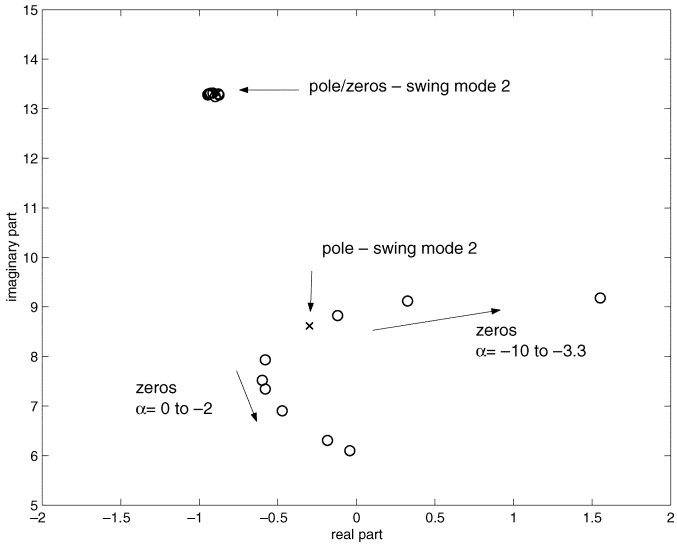

Fig. 9. Zero locations : SSSC in line 5-4.

We first validate the results relating to zero locations by considering the pole–zero locations near the swing frequencies, for the dual input-output pairs corresponding to various devices. The interleaving of the imaginary part of poles corresponding to swing modes, and zeros is clearly seen in all cases (see Fig. 8).

Now consider a SSSC connected in branch 5-4. The pole zero locations with $y = I$ and $u = V_R$ are shown in Fig. 9. We also consider a modified signal with $y' = I - \alpha V_R$. The value of α is *tuned* so as to obtain good pole-zero separation. The better eigenvalue movement with a damping controller using the control law $u(s) = -(ks/(0.01s+1)^2)y'(s)$, using a well tuned value of α, is clearly seen in Fig. 10.

This is verified for a simulation of the system for a self-clearing fault at bus 5, with clearing time of 0.15 s. The range of the injected voltage by the SSSC is assumed to be ± 0.15 p.u. The better performance for the same controller gain, with an appropriate value of α, is clearly seen in Fig. 11.

We now turn our attention to the duality result. For series reactive voltage and shunt real power devices, the modal controllability and observability magnitudes and their ratio are shown

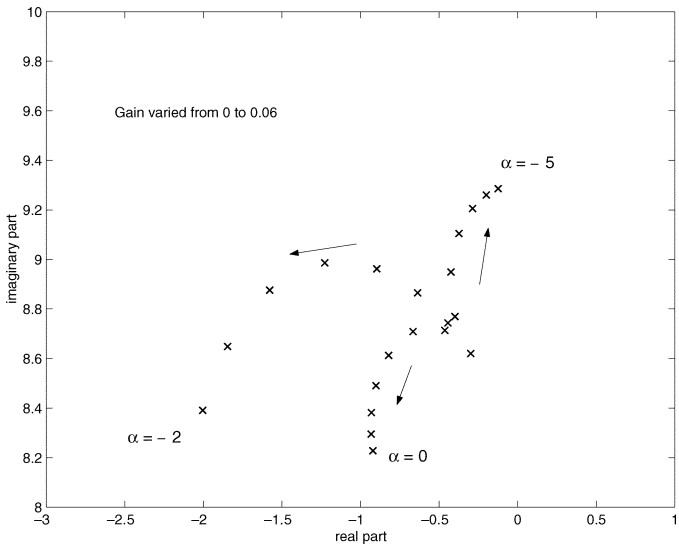

Fig. 10. Root loci with different α : SSSC in line 5-4.

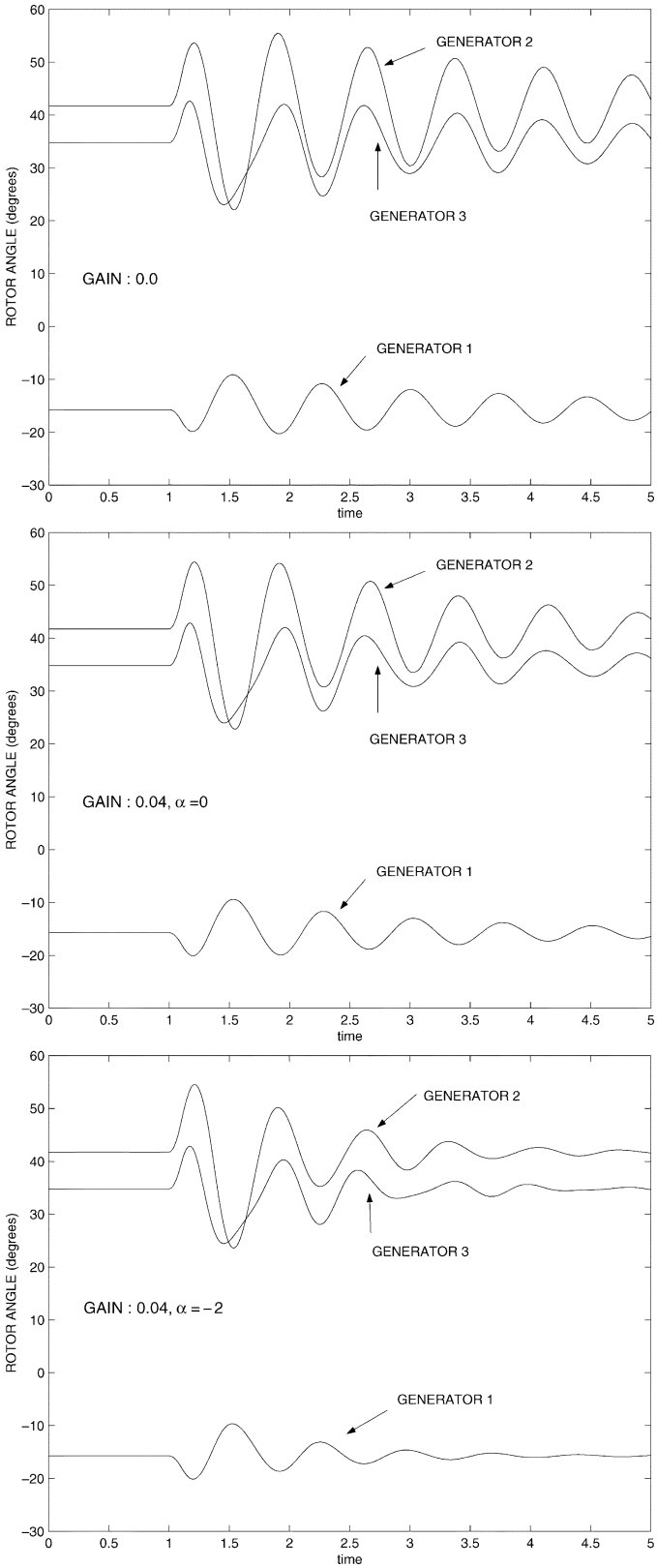

Fig. 11. Response of generator angles for fault: SSSC in line 5-4.

in Tables II and III. The critical nodes/lines selected based on modal observability and controllability are identical and are shown in bold. Therefore, the use of modal observability in ϕ and I to screen candidate locations for shunt real power and series reactive power devices is justified. It is also observed

TABLE II
MODAL CONTROLLABILITY, OBSERVABILITY, AND RESIDUE ANGLE-**DETAILED MODEL** INPUT : P_{sh}, OUTPUT : ϕ

	$\lambda_1 = -0.89 + j13.29$			$\lambda_2 = -0.30 + j8.59$		
Bus	$\lvert\beta_1\rvert$	$\lvert\gamma_1\rvert$	$\angle\rho_1$	$\lvert\beta_2\rvert$	$\lvert\gamma_2\rvert$	$\angle\rho_2$
1	0.620	0.0037	-82	0.359	0.0135	-118
2	1.495	0.0117	-113	**3.566**	**0.1454**	**-79**
3	**8.316**	**0.0533**	**-91**	2.600	0.1008	-85
4	1.421	0.0085	-86	0.616	0.0223	-76
5	1.226	0.0070	-72	1.492	0.0542	-90
6	2.866	0.0182	-101	1.298	0.0471	-88
7	0.748	0.0051	-17	**2.970**	**0.1150**	**-86**
8	2.734	0.0171	-87	**2.806**	**0.1057**	**-90**
9	**5.583**	**0.0362**	**-97**	2.447	0.0929	-88
10	0.998	0.0058	-46	2.260	0.0852	-89

TABLE III
MODAL CONTROLLABILITY, OBSERVABILITY, AND RESIDUE ANGLE-**DETAILED MODEL** INPUT : V_R, OUTPUT : I

	$\lambda_1 = -0.89 + j13.29$			$\lambda_2 = -0.30 + j8.59$		
Branch	$\lvert\beta_1\rvert$	$\lvert\gamma_1\rvert$	$\angle\rho_1$	$\lvert\beta_2\rvert$	$\lvert\gamma_2\rvert$	$\angle\rho_2$
1-4	12.24	0.081	-69	**17.45**	**0.572**	**-75**
4-6	16.39	0.105	-80	7.25	0.265	-86
6-9	16.57	0.100	-70	7.49	0.244	-85
9-3	**50.05**	**0.299**	**-102**	2.67	0.136	-107
9-8	**28.81**	**0.192**	**-71**	3.40	0.123	-76
8-7	**28.49**	**0.190**	**-62**	3.70	0.123	-102
7-2	**34.23**	**0.216**	**-85**	**11.71**	**0.500**	**-110**
10-5	3.03	0.023	-46	9.61	0.370	-95
7-10	3.73	0.024	-78	8.69	0.369	-104
5-4	6.82	0.012	46	9.36	0.216	-54

TABLE IV
MODAL CONTROLLABILITY, OBSERVABILITY, AND RESIDUE ANGLE-**DETAILED MODEL** INPUT : I_R, OUTPUT : V

	$\lambda_1 = -0.89 + j13.29$			$\lambda_2 = -0.30 + j8.59$		
Bus	$\lvert\beta_1\rvert$	$\lvert\gamma_1\rvert$	$\angle\rho_1$	$\lvert\beta_2\rvert$	$\lvert\gamma_2\rvert$	$\angle\rho_2$
1	0.66	0.0004	-35	0.26	0.0010	135
2	**4.94**	**0.0034**	**-57**	**3.46**	0.0041	**-158**
3	**11.2**	**0.0046**	**-141**	1.75	0.0027	-170
4	1.07	0.0004	105	0.61	0.0045	-54
5	0.37	0.0011	99	1.14	**0.0069**	-32
6	3.12	0.0006	-157	0.90	**0.0047**	-39
7	1.46	0.0025	-9.7	**2.50**	0.0027	**-99**
8	2.22	0.0028	178	**2.05**	0.0023	**-101**
9	**7.21**	**0.0038**	**-150**	1.68	0.0020	-133
10	0.72	0.0019	12	1.81	**0.0061**	-39

TABLE V
MODAL CONTROLLABILITY, OBSERVABILITY, AND RESIDUE ANGLE-**DETAILED MODEL** INPUT : P_{ser}, OUTPUT : ζ

	$\lambda_1 = -0.891 + j13.294$			$\lambda_2 = -0.301 + j8.594$		
Branch	$\lvert\beta_1\rvert$	$\lvert\gamma_1\rvert$	$\angle\rho_1$	$\lvert\beta_2\rvert$	$\lvert\gamma_2\rvert$	$\angle\rho_2$
1-4	21.33	0.029	147	**14.70**	**0.383**	**164**
4-6	**77.19**	0.042	177	**13.52**	0.149	-166
6-9	40.51	**0.085**	162	6.93	**0.239**	-173
9-3	**79.80**	0.032	**-60**	3.33	0.043	-72
9-8	**204.86**	**0.187**	**176**	**18.25**	0.065	**-167**
8-7	65.37	0.045	170	7.49	0.165	-148
7-2	35.89	0.012	-64	8.60	0.096	-139
10-5	11.04	0.006	176	9.68	0.136	-151
7-10	10.54	0.004	-125	9.90	0.055	-135
5-4	12.25	**0.048**	143	13.40	**0.517**	127

that for these devices, residue angles lie near -90° for locations with high modal controllability. Moreover, for locations at which both modes have good relative controllability, e.g., nodes 3 and 9 or branches 7-2 and 4-6, the residue angles for both modes are about 10 to 20° apart from -90°, the value predicted by simplified analysis.

The modal observability in V and ζ is not suitable for selecting locations for shunt reactive current and series real power devices (see Tables IV and V). For the higher frequency mode,

although the ratio $|\beta_i/\gamma_i|$ varies significantly with location, the location with largest γ_i and largest β_i coincide. However, this is not true for the interarea mode. This implies that the observability vector alone cannot be used to rank the candidate locations for these devices. Moreover, residue angles for these devices are not in a small range around -90°.

IV. Discussion

A. Zero Locations

Use of signals like local current magnitude in a branch (SSSC) or voltage magnitude at a bus (STATCOM) often results in poles and zeros being close together, even if modal controllability and observability is assured. This results in migration of these poles to the nearby zeros when damping controllers are used with these signals. At least one pair of zeros can be moved away significantly from the poles corresponding to swing modes, by appropriate modification of these local feedback signals. This results in better eigenvalue movement for at least one swing mode when a damping controller is used. Obviously, modes that are not controllable at that location or observable in the local feedback signal will not be affected by the modification. Also, eigenvalue sensitivity at zero gain—the residue—is *not affected* by the modification in feedback signal. Thus, the modification of local feedback signals is useful to obtain good movement for larger gains.

The need for similar feedback signals has been intuitively recognized in the past literature, viz., thevenin voltage signal in [3], voltage across a transmission path in [14], and synthesized angular difference signal in [7].

To show the similarity, consider the modified signal $y' = I - \alpha V_R$ to be used with a SSSC

$$y' = I - \alpha V_R = -\alpha\left(\frac{I}{-\alpha} + V_R\right). \tag{36}$$

This means that $y' \propto IX + V_R$, where $X = 1/-\alpha$. Since α is usually negative, $IX + V_R$ can be interpreted as voltage across the transmission path in which the SSSC is present. This is similar to the signal in [14]. The synthesized angular difference signal across the transmission path [7] also roughly varies in the same way as the voltage across the path for small values of the angular difference. Thus, the analytical result in this paper provides a theoretical justification for use of the synthesized signals proposed in the literature.

Since the linearized matrices are a function of an operating point, σ' will vary depending on the operating point. Consequently, there is a need to "tune" the value of α that is suitable for a wide range of operating conditions.

B. Observability-Based Ranking

The analysis and study of detailed model suggests that modal observability vectors corresponding to ϕ, I, $\Delta I/I_o$ are good measures for ranking/screening of shunt real and series reactive FACTS devices since they correspond quite well with modal controllability-based ranking. While this provides a justification for use of observability-based ranking for certain devices and signals, a natural question which arises is: Is this result of practical use?

Modal observability-based ranking of candidate locations for damping power swings can be more convenient for a large system than modal controllability or residue based ranking, as it can be done on a system without explicitly representing the FACTS damping controller at each candidate location in a computer program. This is not a major issue any longer, given the vast computing power available today. It is, however, conceivable to utilize actual field measurements of disturbances to extract the relative modal observability at various locations and select locations based on these measurements.

C. Choice of Feedback Signals

The main results presented in this paper are specific to the dual input–feedback signal pairs. Therefore, a question comes to mind: How important is this result if it applies only to specific signals? Clearly, a wider choice of feedback signals does exist. However, voltage and current measurements are routinely available and do deserve specific attention. For the dual signals corresponding to shunt real power and series reactive power devices, residue angles lie in a fairly small range near -90° for different swing modes. Therefore, design of a phase compensator for these damping controllers is somewhat simpler, since substantially different phase shifts for each mode are not required.

An interesting corollary of the duality result is that if a mode is poorly observable in ϕ and I at a location, then it is poorly controllable by FACTS devices that modulate P_{sh} and V_R, respectively, at that location. *This implies that "global signals" are of little use for these FACTS devices if modal observability in the dual local signals is poor.*

V. Conclusion

In this paper, we have investigated the properties of zero locations and duality between modal controllability and modal observability when certain local signals are used for FACTS-based damping controllers. It is shown that for certain local signals, zeros are interleaved with open loop poles. Modifications are suggested in the local feedback signals to obtain good pole–zero separation and better eigenvalue movement for damping controllers. The result is demonstrated using SSSC-based damping controllers.

For simple models, there is a duality between modal observability in certain local signals and modal controllability using corresponding FACTS devices. Also, residue angles are the same for different swing modes and locations when dual signals are used for feedback.

Case studies to verify these results using detailed models reveal the following.

1) Relative modal controllability using series reactive and shunt real power modulation-based FACTS devices at various locations can be approximately inferred from the relative modal observability in line current magnitude and bus voltage phase angle at those locations, respectively. Thus, the candidate locations for these devices can be selected based on the relative modal observability of local signals. Use of these feedback signals results in residue angles that are fairly close to each other for different swing modes.

2) For shunt reactive and series real power modulation, modal controllability cannot be inferred from modal observability in bus voltage magnitude or line current phase angle, respectively. A bus with largest modal voltage oscillations *is not necessarily* the location with the largest controllability using shunt reactive power devices. Thus, the observability vector cannot be used to reliably rank the candidate locations for these devices.

If modal controllability at a particular location is smaller, a larger controllable range (equivalently a larger equipment size and cost) is required to obtain a specified damping performance for a given disturbance. Further work is required to obtain a more precise and quantitative relationship between disturbance magnitude, damping performance, and the required controllable range. This will help a system planner to assess the cost and utility of FACTS options for damping power swings.

APPENDIX
FORMATION OF THE STATE EQUATION

The electromechanical modes in a system are highlighted by considering the classical model of generators. The assumptions given in Section II are applicable here.

At any bus j (not the generator internal bus), the injected power P_{shj} by a FACTS controller is given by

$$P_{shj} = P_{Lj} + \sum_{i\in n_j} \frac{V_j V_i}{x_{ij}} \sin(\phi_j - \phi_i) + \sum_{k\in m_j} \frac{V_j E_k}{x'_{dk}} \sin(\phi_j - \phi_k) + \sum_{l\in r_j} V_j I_l \cos(\phi_j - \zeta) S_{lj} \quad (37)$$

where n_j is set of buses connected to bus j by a transmission line, m_j is the set of generator (internal) buses connected to bus j, and r_j is the set of branches where series FACTS controllers are connected. P_{Lj} is the power consumed by the load connected at bus j. x_{ij} is the reactance of the transmission line connecting bus i and j. x'_{dk} is the transient reactance of generator k.

$S_{lj} = 1$ if the reference direction of current in the lth branch is outward from the jth node; $S_{lj} = -1$ otherwise.

At the kth generator internal bus, injected power is given by

$$P_{ek} = \frac{E_k V_j \sin(\delta_k - \phi_j)}{x'_{dk}}. \quad (38)$$

The reactive current balance equation at the jth node can be written as follows:

$$I_{Rj} = -V_j b_{shj} + \sum_{i\in n_j} \frac{V_j}{x_{ij}} - \frac{V_i \cos(\phi_j - \phi_i)}{x_{ij}} + \sum_{k\in m_j} \frac{V_j}{x'_{dk}} - \frac{V_j}{x'_{dk}} \cos(\delta_j - \phi_k) + \sum_{l\in r_j} I_l \sin(\phi_j - \zeta) S_{lj} \quad (39)$$

where b_{shj} is the fixed shunt susceptance at the jth bus. For the lth branch (connected between nodes F_l and T_l), where a series FACTS controller is present (see Fig. 12), the real power and reactive voltage balance equations are given by

$$P_{serl} = -V_{Fl} I_l \cos(\phi_{Fl} - \zeta) + V_{Tl} I_l \cos(\phi_{Tl} - \zeta) \quad (40)$$

$$V_{Rl} = (V_{Fl} \sin(\phi_{Fl} - \zeta) - V_{Tl} \sin(\phi_{Tl} - \zeta)). \quad (41)$$

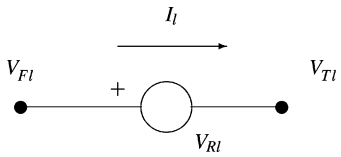

Fig. 12. Branch with reactive voltage compensation.

The *linearized* real power and reactive power balance equations can be written as

$$\begin{bmatrix} \mathbf{\Delta P_e} \\ \mathbf{\Delta P_{sh}} \\ \mathbf{\Delta I_R} \\ \mathbf{\Delta P_{ser}} \\ \mathbf{\Delta V_R} \end{bmatrix} = \begin{bmatrix} A_{11} & A_{12} & A_{13} & A_{14} & A_{15} \\ A_{21} & A_{22} & A_{23} & A_{24} & A_{25} \\ A_{31} & A_{32} & A_{33} & A_{34} & A_{35} \\ A_{41} & A_{42} & A_{43} & A_{44} & A_{45} \\ A_{51} & A_{52} & A_{53} & A_{54} & A_{55} \end{bmatrix} \begin{bmatrix} \mathbf{\Delta\delta} \\ \mathbf{\Delta\phi} \\ \mathbf{\Delta V} \\ \mathbf{\Delta\zeta} \\ \mathbf{\Delta I} \end{bmatrix}. \quad (42)$$

Note that $\Delta P_L = 0$, since constant power loads are considered.

The elements of the various submatrices are defined as

$$A_{11}(i,j) = \frac{\partial P_{ei}}{\partial \delta_j} \quad A_{12}(i,j) = \frac{\partial P_{ei}}{\partial \phi_j} \quad A_{13}(i,j) = \frac{\partial P_{ei}}{\partial V_j}$$
$$A_{14}(i,j) = \frac{\partial P_{ei}}{\partial \zeta_j} \quad A_{15}(i,j) = \frac{\partial P_{ei}}{\partial I_j} \quad A_{21}(i,j) = \frac{\partial P_{shi}}{\partial \delta_j}$$
$$A_{22}(i,j) = \frac{\partial P_{shi}}{\partial \phi_j} \quad A_{23}(i,j) = \frac{\partial P_{shi}}{\partial V_j} \quad A_{24}(i,j) = \frac{\partial P_{shi}}{\partial \zeta_j}$$
$$A_{25}(i,j) = \frac{\partial P_{shi}}{\partial I_j} \quad A_{31}(i,j) = \frac{\partial I_{Ri}}{\partial \delta_j} \quad A_{32}(i,j) = \frac{\partial I_{Ri}}{\partial \phi_j}$$
$$A_{33}(i,j) = \frac{\partial I_{Ri}}{\partial V_j} \quad A_{34}(i,j) = \frac{\partial I_{Ri}}{\partial \zeta_j} \quad A_{35}(i,j) = \frac{\partial I_{Ri}}{\partial I_j}$$
$$A_{41}(i,j) = \frac{\partial P_{seri}}{\partial \delta_j} \quad A_{42}(i,j) = \frac{\partial P_{seri}}{\partial \phi_j} \quad A_{43}(i,j) = \frac{\partial P_{seri}}{\partial V_j}$$
$$A_{44}(i,j) = \frac{\partial P_{seri}}{\partial \zeta_j} \quad A_{45}(i,j) = \frac{\partial P_{seri}}{\partial I_j} \quad A_{51}(i,j) = \frac{\partial V_{Ri}}{\partial \delta_j}$$
$$A_{52}(i,j) = \frac{\partial V_{Ri}}{\partial \phi_j} \quad A_{53}(i,j) = \frac{\partial V_{Ri}}{\partial V_j} \quad A_{54}(i,j) = \frac{\partial V_{Ri}}{\partial \zeta_j}$$
$$A_{55}(i,j) = \frac{\partial V_{Ri}}{\partial I_j}.$$

From (37)–(41), it is evident that the matrix in (42) is *symmetric*.

The swing equations for generator k can be expressed as

$$M_k \frac{d^2\delta_k}{dt^2} = P_{mk} - P_{ek}, \quad k = 1,2\ldots n_g. \quad (43)$$

On linearizing the swing equations, we obtain

$$M_k \frac{d^2\Delta\delta_k}{dt^2} = \Delta P_{mk} - \Delta P_{ek} = -\Delta P_{ek}. \quad (44)$$

Note that $\Delta\omega = d\Delta\delta/dt$, $\Delta P_{mk} = 0$, and n_g is the number of generators.

Thus, from (42) and (44), we obtain (1).

REFERENCES

[1] N. Hingorani and L. Gyugyi, *Understanding FACTS*. New York: IEEE Press, 2000.

[2] L. Anquist, B. Lundin, and J. Samuelsson, "Power oscillation damping using controlled reactive power compensation : A comparison between series and shunt approaches," *IEEE Trans. Power Syst.*, vol. 8, no. 2, pp. 687–699, May 1993.

[3] E. V. Larsen, K. Clark, A. T. Hill, R. J. Piwko, M. J. Beshir, M. Bhuiyan, F. J. Hormozi, and K. Braun, "Control design for SVC's on the Mead-Adelanto and Mead-Phoenix transmission project," *IEEE Trans. Power Del.*, vol. 11, no. 3, pp. 1498–1506, Jul. 1996.

[4] B. Chaudhuri and B. C. Pal, "Robust damping of multiple swing modes employing global stabilizing signals with a TCSC," *IEEE Trans. Power Syst.*, vol. 19, no. 1, pp. 499–506, Feb. 2004.

[5] M. Aboul-Ela, A. Sallam, J. McCalley, and A. Fouad, "Damping controller design for power system oscillations using global signals," *IEEE Trans. Power Syst.*, vol. 11, no. 2, pp. 767–773, May 1996.

[6] L. Jones and G. Andersson, "Application of modal analysis of zeros to power system control and stability," *Elsevier Elect. Power Syst. Res.*, vol. 46, no. 3, pp. 205–211, 1998.

[7] E. V. Larsen, J. J. Sanchez-Gasca, and J. H. Chow, "Concepts for design of FACTS controllers to damp power swings," *IEEE Trans. Power Syst.*, vol. 10, no. 2, pp. 948–955, May 1995.

[8] N. Martins and L. T. G. Lima, "Determination of suitable location for power system stabilizers and static var compensators for damping electromechanical oscillations in large scale systems," *IEEE Trans. Power Syst.*, vol. 5, no. 4, pp. 1455–1469, Nov. 1990.

[9] D. Miu, *Mechatronics, Electromechanics and Contromechanics*. New York: Springer-Verlag, 1993.

[10] O. Samuelsson, ""Load modulation for damping of electro-mechanical oscillations," Panel paper," in *Proc. IEEE Power Eng. Soc. Winter Meeting*, Columbus, OH, Jan.-Feb. 28–1, 2001.

[11] G. H. Golub and C. F. Van Loan, *Matrix Computations*, 2nd ed. Baltimore, MD: The John Hopkins Univ. Press, 1989, pp. 589–590.

[12] P. M. Anderson and A. A. Fouad, *Power System Control and Stability*. Ames, IA: Iowa State Univ. Press, 1977.

[13] K. R. Padiyar, *Power System Dynamics—Stability and Control*, 2nd ed. Hyderabad, India: B.S.Publications, 2002.

[14] A. M. Kulkarni and K. R. Padiyar, "Damping of power swings using series facts controllers," *Int. J. Elect. Power Energy Syst.*, vol. 21, no. 7, pp. 475–495, Oct. 1999.

U. P. Mhaskar received the B.E. and M.E. degrees in electrical engineering from Walchand College of Engineering, Sangli, India, and the Ph.D. degree from Indian Institute of Technology, Bombay, India, in 2004.

At present, he is employed at GE India Technology Center, Bangalore, India. His interests include FACTS, power system modeling, and simulation

A. M. Kulkarni received the B.E. degree in electrical engineering from University of Roorkee, Roorkee, India, in 1992, and the ME degree in electrical engineering in 1994 and the Ph.D. degree in 1998 from Indian Institute of Science, Bangalore, India.

He is currently an Assistant Professor at Indian Institute of Technology, Bombay, India. His research interests include power system dynamics and FACTS.